Tuning of Synchronous-Frame PI Current Controllers in Grid-Connected Converters Operating at a Low Sampling Rate by MIMO Root Locus

Fernandez, Francisco Daniel Freijedo; Vidal, Ana; Yepes, Alejandro G.; Guerrero, Josep M.; Lopez, Oscar; Malvar, Jano; Doval-Gandoy, Jesus

Published in:
I E E E Transactions on Industrial Electronics

DOI (link to publication from Publisher):
10.1109/TIE.2015.2402114

Publication date:
2015

Document Version
Early version, also known as pre-print

This article has been accepted for publication in a future issue of this journal, but has not been fully edited. Content may change prior to final publication. Citation information: DOI 10.1109/TIE.2015.2402114, IEEE Transactions on Industrial Electronics

Tuning of Synchronous-Frame PI Current Controllers in Grid-Connected Converters Operating at a Low Sampling Rate by MIMO Root Locus

Francisco D. Freijedo, Ana Vidal, *Student Member, IEEE*, Alejandro G. Yepes, *Member, IEEE*, Josep M. Guerrero, *Fellow Member, IEEE*, Óscar López, *Member, IEEE*, Jano Malvar, *Student Member, IEEE* and Jesús Doval-Gandoy, *Member, IEEE*

***Abstract*—Current controller performance is key in grid-connected power converters for renewable energy applications. In this context, a challenging scenario is arising in multi-MW wind turbines, where sampling and switching frequencies tend to be lower and lower as power ratings increase. This strongly affects achievable control time constant. With this perspective, this paper presents a systematic procedure for accurate dynamics assessment and tuning of synchronous-frame PI current controllers, which is based on linear control for multiple input multiple output (MIMO) systems. The dominant eigenvalues of the system are calculated with explicit consideration of time-delay and cross-coupling terms, two factors which clearly impair the system dynamics when considering a low sampling frequency. The proposed methodology is summarized as follows. Firstly, the plant and controller matrices are modeled in state-space. Subsequently, the characteristic polynomial of the closed-loop system is obtained and a computer-aided parametric analysis is performed to calculate the MIMO root locus as a function of the control gain. By its inspection, it is possible to identify the gain which minimizes the current closed-loop time constant. This tuning is suitable for wind turbine applications, taking into consideration cascaded-control structures and grid-code requirements. The validity and accuracy of the analysis is fully supported by experimental verification.**

***Index Terms*—Ac/dc power conversion, current control, pulse width modulation converters, wind power generation.**

I. Introduction

Synchronous-frame proportional-integral (dq-PI) current controllers are widely employed in ac drives [1]–[3] and grid-tied converters [4], [5]. The synchronous-frame axes d and q rotate at the angular frequency ω of voltage/current waveforms. From the control point of view, this is advantageous since ac voltages/currents are controlled by dc variables, so PI regulators provide their highest performance. In this manner, dq-PI current controllers achieve reference tracking and disturbance rejection with zero steady-state error [1]–[7].

In addition to steady-state features, time-domain dynamics are also very important in some grid-connected applications, such as wind turbines. When cascaded controllers are implemented, special care must be put on tuning the innermost current loops, as they establish the dynamic performance of the overall system (i.e., inner loops should be much faster than the outer loops) [6], [8]–[10]. Furthermore, some grid codes also demand stringent time-domain dynamics in terms of reference tracking when a fault is detected, forcing generation units to supply a certain amount of reactive current within a specific response time [8], [11]. Fulfilling these requirements becomes challenging in a multi-MW context, where switching and sampling frequencies tend to be very low [12], [13].

Closed-loop dynamics mainly depends on the controller gains, so the tuning process is key to optimize the current control loop behavior. Ideally, the PI gains can be tuned so that the system is defined by a single dominant pole, which is set by the controller gain [1], [2] (this gain sets the closed-loop bandwidth, so the term "bandwidth gain" is employed in this paper). However, real systems may differ from ideal ones mainly due to parameter deviations [1], [2] and time-delay effects [3], [7]. Fine analysis for high-bandwidth tuning optimization requires to include the time delay in the circuit modeling [3], [7], [14]–[17].

A big shortcoming of dq-PI controllers arises when considering both the time-delay and the (cross-coupling) decoupling schemes at the same time. The classical dq-PI with feedback axes-decoupling presents important remaining cross-channel effects [14]–[17]. On the other hand, cross-coupling terms are usually neglected for tuning the controllers, so the dq-PI system with delays can be approximated to a second order single-input single-output (SISO) loop [3], [18]. Even though these approaches give useful guidelines for the control parameters, they dismiss cross-coupling effects in the dynamics (root-locus trajectories also depend on cross-coupling terms). The influence of cross-coupling terms in the system dynamics have been previously reported in electric drives applications with high ratios of fundamental-to-sampling frequencies [14]–[17]. Therefore, coupling should be also considered in the grid-connected converters when low sampling frequencies are considered.

Manuscript received August 3, 2014; revised November 25, 2014 and December 30, 2014; accepted January 13, 2015.

This work was supported in part by the Energinet Forskel program under the project PSO-2014-1-12188 and in part by the Spanish Ministry of Science and Innovation and by the European Commission (European Regional Development Fund) under the project DPI2012-31283.

Francisco D. Freijedo and Josep M. Guerrero are with the Department of Energy Technology, Aalborg University, 9220 Aalborg East, Denmark (e-mail: {fran,joz}@et.aau.dk).

Ana Vidal, Alejandro G. Yepes, Óscar López, Jano Malvar and Jesús Doval-Gandoy are with the Department of Electronics Technology, University of Vigo, Vigo, Spain (e-mail: {anavidal,agyepes,olopez,janomalvar,jdoval}@uvigo.es).

This article has been accepted for publication in a future issue of this journal, but has not been fully edited. Content may change prior to final publication. Citation information: DOI 10.1109/TIE.2015.2402114, IEEE Transactions on Industrial Electronics

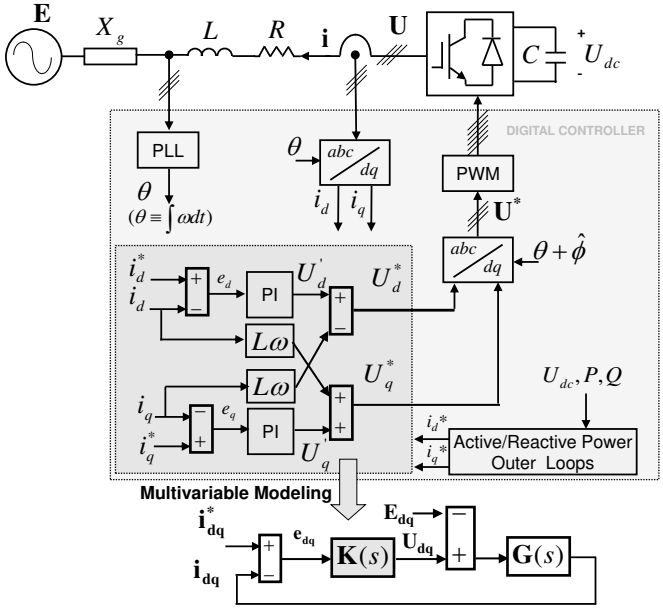

Fig. 1. MIMO current control problem for a grid-connected power converter.

This paper contributes a systematic procedure for accurate assessment and tuning of the classic dq-PI current controllers dynamics, which is based on linear control for multivariable, or multiple input multiple output (MIMO), systems. The effect of non-diagonal components, due to remaining cross couplings associated to the system time-delay, is explicitly considered. The MIMO characteristic polynomial is obtained from an accurate modeling of the plant and control matrices, which define the MIMO sensitivities. Its roots (eigenvalues) determine the system closed-loop dynamics [19], [20]. These roots depend on the controller tuning (bandwidth gain). From a given design objective the tuning is obtained. In this work, the design aim is to minimize the current loop time constant, as it provides a good trade-off considering both cascading controllers dynamics [6], [8], [9] and transient response for grid-code compliance [8], [11].

The rest of the paper is organized as follows. Section II shows a basic background in modeling and control from reference papers. Section III develops the plant modeling with explicit consideration of delays, which gives rise to a non-diagonal plant transfer function with explicit time-delay terms. Section IV analyzes a simplified second order standard system, obtained by neglecting coupling terms. The main aim of this section is to provide a qualitative description of the closed-loop dynamics and support the assumptions made in the next section. Section V develops the MIMO method for an accurate calculation (as it includes coupling terms) of system eigenvalues, and shows how to identify the pair of dominant poles by inspection of MIMO root locus diagrams. Section VI provides experimental support to the theoretical approach. The key experimental results prove the higher accuracy provided by the MIMO based approach.

II. Background

Fig. 1 represents a power converter connected to the grid and its discrete controller based on a dq-PI with feedback decoupling implementation [1]. By assuming a stiff grid, i.e., $|X_g| << L\omega$ [21], [22], the state-space equation of the power circuit (plant) is given by

$$\frac{d}{dt}\begin{bmatrix} i_d(t) \\ i_q(t) \end{bmatrix} = \begin{bmatrix} -R/L & \omega \\ -\omega & -R/L \end{bmatrix}\begin{bmatrix} i_d(t) \\ i_q(t) \end{bmatrix} + \\ + \frac{1}{L}\mathbf{I}\begin{bmatrix} U_d(t) \\ U_q(t) \end{bmatrix} - \frac{1}{L}\mathbf{I}\begin{bmatrix} E_d(t) \\ E_q(t) \end{bmatrix} \tag{1}$$

with

$$\mathbf{I} \equiv \begin{bmatrix} 1 & 0 \\ 0 & 1 \end{bmatrix}. \tag{2}$$

Equation (1) has cross-coupling terms as a result of the Park transforms [1], [7]. A classical decoupling strategy is given by the following change of variable in the control action [1]:

$$\begin{bmatrix} U_d^*(t) \\ U_q^*(t) \end{bmatrix} = \mathbf{I}\begin{bmatrix} U_d'(t) \\ U_q'(t) \end{bmatrix} + \begin{bmatrix} 0 & -L\omega \\ L\omega & 0 \end{bmatrix}\begin{bmatrix} i_d(t) \\ i_q(t) \end{bmatrix}. \tag{3}$$

If the system time delays due to discrete operation and PWM blocks are neglected (see Fig. 1):

$$\begin{bmatrix} U_d(t) \\ U_q(t) \end{bmatrix} = \begin{bmatrix} U_d^*(t) \\ U_q^*(t) \end{bmatrix}. \tag{4}$$

By substituting (4) in (1), the "effective plant" is given by the following diagonal (decoupled) system:

$$\frac{d}{dt}\begin{bmatrix} i_d(t) \\ i_q(t) \end{bmatrix} = \frac{-R}{L}\mathbf{I}\begin{bmatrix} i_d(t) \\ i_q(t) \end{bmatrix} + \frac{1}{L}\mathbf{I}\begin{bmatrix} U_d'(t) \\ U_q'(t) \end{bmatrix} - \frac{1}{L}\mathbf{I}\begin{bmatrix} E_d(t) \\ E_q(t) \end{bmatrix}. \tag{5}$$

From (5), the plant matrix transfer function $\mathbf{G}(s)$ is given by

$$\mathbf{i}(s)|_{\mathbf{E}(s)=0} = \underbrace{\frac{1}{L(s+R/L)}\mathbf{I}}_{\mathbf{G}(s)} \cdot \mathbf{U}(s). \tag{6}$$

This plant modeling should be reconsidered to include the effect of grid impedance when the stiff assumption is not realistic, that is in weak grids [21], [22]. In such a situation, a grid inductive part L_g should be added to L to give the total system inductance and a grid resistive part R_g should be added to R to give the total system resistance [23], [24]. On the other hand, Fig. 1 is also suitable to describe induction motor drives [3]. In that case, both the motor and converter filter impedances should be included in the model [3].

After plant transfer modeling by (6), a diagonal PI controller according to the internal model laws [1], [2], [25] is defined as

$$\mathbf{K}(s) = \frac{\alpha L(s+R/L)}{s}\mathbf{I} \tag{7}$$

with α being the bandwidth gain, and assuming a good knowledge of the filter parameters. $\mathbf{G}(s)\mathbf{K}(s) = \alpha/s\mathbf{I}$ is the resulting open-loop transfer function matrix. When the closed loop is considered, the time constant is the inverse of α [1], [7]. Since it is a first order diagonal system, each channel is independent from each other, and the control problem is reduced to two independent SISO loops. Such a simple analysis is only accurate for a limited range of α values. In

This article has been accepted for publication in a future issue of this journal, but has not been fully edited. Content may change prior to final publication. Citation information: DOI 10.1109/TIE.2015.2402114, IEEE Transactions on Industrial Electronics

high-bandwidth systems, this first order approximation does not provide reliable information about time response, damping or stability [3]. In practice, it is assumed that α should be ten times smaller than the sampling frequency f_s [1], [7]. However, second order features (e.g., overshoot) are noticeable for bandwidth gains even smaller than one-tenth of f_s [3], [7]. Therefore, as time-delay effects are considered, the dynamics is better defined by second order systems [3], [7], [15]–[17].

III. Multivariable Plant Modeling with Time-Delay Consideration

This section details the system modeling taking into account the controller delay. This has relevant effects in the closed-loop dominant roots, as previously discussed.

A time delay t_d due to discrete-time operation and PWM is considered. The value of t_d is given by

$$t_d = 1.5/f_s, \tag{8}$$

one sample due to discrete-time operation added to half a sample associated to the PWM operation [3], [7], [16]. Thus, the converter output voltage is rewritten as

$$\begin{bmatrix} U_d(t) \\ U_q(t) \end{bmatrix} = \mathbf{\Phi}_{lag} \begin{bmatrix} U_d^*(t-t_d) \\ U_q^*(t-t_d) \end{bmatrix} \tag{9}$$

with

$$\mathbf{\Phi}_{lag} = \begin{bmatrix} \cos(\phi) & \sin(\phi) \\ -\sin(\phi) & \cos(\phi) \end{bmatrix} \tag{10}$$

and

$$\phi = t_d \omega \tag{11}$$

being a rotation matrix and its corresponding angle, respectively. These expressions have an insightful physical meaning. The output voltages (control action) in the synchronous frame are delayed t_d (as in stationary frame analysis [3], [7]), but also rotate an angle ϕ in relation to its reference vector (inputs of the PWM block) [16].

To compensate these effects, a phase-angle lead $\hat{\phi}$ is included in the inverse Park-transform before the modulation block (see Fig. 1) [7], [16], [17]. This delay-compensation technique can be modeled as

$$\begin{bmatrix} U_d(t) \\ U_q(t) \end{bmatrix} = \mathbf{\Phi}_{lead}\mathbf{\Phi}_{lag} \begin{bmatrix} U_d^*(t-t_d) \\ U_q^*(t-t_d) \end{bmatrix} \tag{12}$$

with

$$\mathbf{\Phi}_{lead} = \begin{bmatrix} \cos(\hat{\phi}) & -\sin(\hat{\phi}) \\ \sin(\hat{\phi}) & \cos(\hat{\phi}) \end{bmatrix} \tag{13}$$

and

$$\hat{\phi} = \hat{t}_d \hat{\omega} \tag{14}$$

being the delay-compensation matrix and the estimated delay angle, respectively. It is straightforward to notice that an accurate estimation of the delay angle results in $\mathbf{\Phi}_{lead}$ that equals $\mathbf{\Phi}_{lag}^{-1}$ and, therefore $\mathbf{\Phi}_{lead}\mathbf{\Phi}_{lag} = \mathbf{I}$. The control action is then simplified to

$$\begin{aligned} \begin{bmatrix} U_d(t) \\ U_q(t) \end{bmatrix} = \begin{bmatrix} U_d^*(t-t_d) \\ U_q^*(t-t_d) \end{bmatrix} = \mathbf{I} \begin{bmatrix} U_d'(t-t_d) \\ U_q'(t-t_d) \end{bmatrix} + \\ + \begin{bmatrix} 0 & -L\omega \\ L\omega & 0 \end{bmatrix} \begin{bmatrix} i_d(t-t_d) \\ i_q(t-t_d) \end{bmatrix}. \end{aligned} \tag{15}$$

As seen, besides its positive effect in dynamics [7], [16], [17], the delay compensation simplifies the theoretical analysis.

Subsequently, time-domain expressions should be transformed to the frequency-domain. A first order Padé approximation of the time-shifting property is given by

$$\begin{aligned} \mathcal{L}(f(t-t_d)) = f(s)\cdot e^{-st_d} = f(s)\cdot \frac{e^{-\frac{t_d s}{2}}}{e^{\frac{t_d s}{2}}} \approx \\ \approx f(s)\cdot \frac{-\frac{t_d}{2}s+1}{\frac{t_d}{2}s+1} = f(s)\cdot \frac{-s+2/t_d}{s+2/t_d} \end{aligned} \tag{16}$$

which is very accurate at frequencies one decade below $1/t_d$, i.e., at the expected bandwidth values [1], [7], [18]. Taking into account this property, (15) is converted to the frequency domain and substituted in (1). Thus, the power converter state-space model results in

$$\begin{aligned} s\begin{bmatrix} i_d(s) \\ i_q(s) \end{bmatrix} = \begin{bmatrix} -R/L & \frac{2\omega s}{s+2/t_d} \\ -\frac{2\omega s}{s+2/t_d} & -R/L \end{bmatrix} \begin{bmatrix} i_d(s) \\ i_q(s) \end{bmatrix} + \\ + \frac{-s+2/t_d}{L(s+2/t_d)}\mathbf{I}\begin{bmatrix} U_d'(s) \\ U_q'(s) \end{bmatrix} - \frac{1}{L}\mathbf{I}\begin{bmatrix} E_d(s) \\ E_q(s) \end{bmatrix}. \end{aligned} \tag{17}$$

It should be noted that there are still coupling terms due to time-delay effects in the decoupling paths [16], [17]. Then, from (17), the equivalent plant transfer function is given by

$$\begin{aligned} \mathbf{G}(s) = \frac{-s+2/t_d}{L[(s+R/L)^2(s+2/t_d)^2+4\omega^2 s^2]}\cdot \\ \cdot \begin{bmatrix} (s+R/L)(s+2/t_d) & -2\omega s \\ 2\omega s & (s+R/L)(s+2/t_d) \end{bmatrix}. \end{aligned} \tag{18}$$

Thus, in spite of axes-decoupling and delay-compensation schemes, the effective plant still depends on the time delay.

It is interesting to mention that (18) is in agreement with previous works in the field of electric drives, as it shows a coupling dependence with ω [15]–[17].

A. Accuracy of the Time-Delay Rational Approximation

Linear control system with delays can be accurately assessed by S-domain analysis methods in the range of frequencies at which the rational approximations of time delays are accurate [19], [20]. In this work, (16) approximates the system delay by a rational function of first order. This approach implicitly assumes its accuracy in the range of frequencies at which the control acts, i.e., the control bandwidth, which is assumed to be limited according to the one-to-tenth rule: $\alpha \leq 2\pi f_s/10$ [1], [7]. Fig. 2(a) proves the accuracy of this assumption, as the rational function (modeled in the S-domain) perfectly matches a one sampling delay (modeled in the Z-domain) in the bandwidth range of frequencies. Fig. 2(b) shows the accuracy of the rational approximation in the time-domain by its step response. The rational expression has an initial undershoot and then needs around three samples to track the delayed signal [19].

This article has been accepted for publication in a future issue of this journal, but has not been fully edited. Content may change prior to final publication. Citation information: DOI 10.1109/TIE.2015.2402114, IEEE Transactions on Industrial Electronics

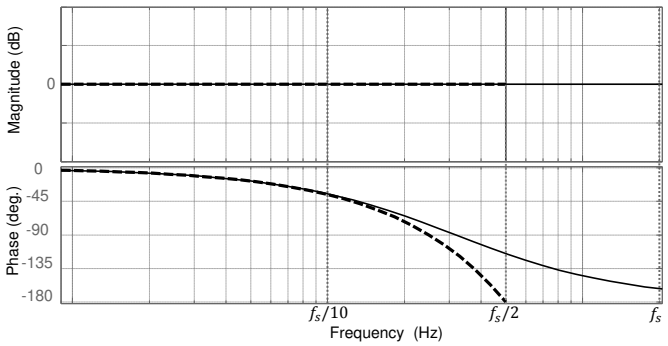

(a)

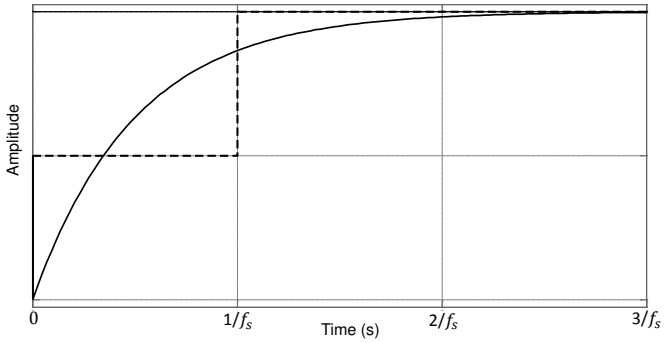

(b)

Fig. 2. Accuracy of first order rational approximation of time delays. Solid: first order rational approximation ($D(s) = e^{s/f_s} \approx \frac{1-s/2f_s}{1+s/2f_s}$). Dotted: one sample delay in the Z-domain ($D(z) = 1/z$). (a) Frequency-domain response; (b) Time-domain unit step response.

IV. Dynamics Assessment and Tuning by a SISO Root-Locus Approximation

The multivariable system can be approximated to two independent second order SISO systems by simply neglecting the coupling terms in (18), so that $\mathbf{G}(s)$ becomes diagonal [26]. Under this assumption, the open-loop transfer function is

$$\mathbf{G}(s)\mathbf{K}(s) = \frac{\alpha(-s+2/t_d)}{s(s+2/t_d)}\mathbf{I}. \tag{19}$$

The non-minimum phase zero at the numerator accurately represents a negative impact due to the system delays, as shown below. This expression, and hence the subsequent SISO analysis, can be also obtained by assuming a first order Padé approximation in the open-loop transfer function analyzed in [3]. From (19), the closed-loop dynamics in the presence of current reference changes is given by

$$\mathbf{T}(s) = \frac{\alpha(-s+2/t_d)}{s^2+(2/t_d-\alpha)s+2\alpha/t_d}\mathbf{I}. \tag{20}$$

A. SISO Root Locus

From (19), it is possible to calculate the eigenvalues of (20), as a function of α, by the SISO root-locus method [27]. Fig. 3 represents the SISO root-locus diagram of the system given by (19)-(20). The closed-loop poles evolve from the open-loop poles at $-2/t_d$ and 0 (at low α values) through the system non-minimum phase zeros at $+2/t_d$ and ∞ [27]; i.e.,

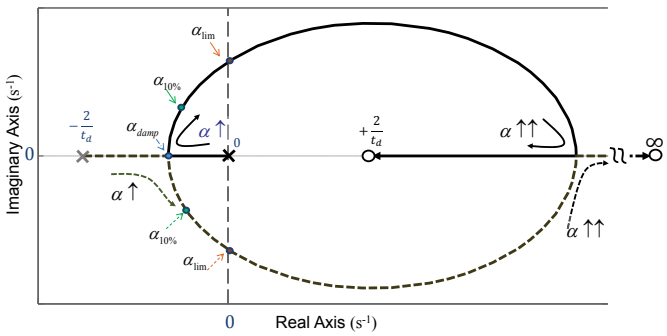

Fig. 3. SISO root locus from (19). Solid: trajectory of p_1. Dashed: trajectory of p_2. Key α tuning values are highlighted.

as α increases, the non-minimum phase zeros (due to system delays) "attract" the closed-loop poles to the unstable plane.

1) Identification of Dominant Time Constants: For low α values, p_1 is closer to the right half plane (RHP), and hence its dynamics is slower than the one given by p_2. In such a case, it is possible to neglect the effect of p_2 and consider $p_d = p_1$ as a single dominant eigenvalue. Hence, the dynamics of the system is well defined by a single order system, for which the time constant is

$$\tau = \frac{1}{|\Re\{p_d\}|}. \tag{21}$$

At a certain α p_1 and p_2 converge and then, for larger α values, the system is defined by a pair of complex eigenvalues, such that $p_1 = p_2^*$. As they dominate the system dynamics, the pair of complex eigenvalues can be referred to $p_{d_{1,2}} = [p_{d1}, p_{d1}^*]$. The dynamics of a second order system is usually defined as a function of the standard parameters

$$\begin{aligned} \omega_n &= \sqrt{\Re^2\{p_{d1}\}+\Im^2\{p_{d1}\}} \quad \text{(natural frequency)} \\ \xi &= \frac{\Re\{p_{d1}\}}{\sqrt{\Re^2\{p_{d1}\}+\Im^2\{p_{d1}\}}} \quad \text{(damping ratio).} \end{aligned} \tag{22}$$

Now, (20) can be written as a standard second order transfer function as

$$\mathbf{T}(s) = \frac{\omega_n^2(1-st_d/2)}{s^2+2\xi\omega_n s+\omega_n^2}\mathbf{I} \tag{23}$$

with

$$\begin{aligned} \omega_n &= \sqrt{2\alpha/t_d} \quad \text{(natural frequency)} \\ \xi &= \frac{2/t_d-\alpha}{2\sqrt{2\alpha/t_d}} \quad \text{(damping ratio).} \\ [t_d &= 2/\omega_n(\sqrt{1+\xi^2}-\xi)]. \end{aligned} \tag{24}$$

It should be noted that the non-minimum phase zero can be kept as function of t_d (for the sake of clarity, as it does not change with α), but also as a function of the standard parameters (ω_n and ξ). The time constant of a standard second order system is given by

$$\tau = \frac{1}{\xi\omega_n} = \frac{1}{|\Re\{p_{d1}\}|}. \tag{25}$$

The settling time to within a tolerance band of the 2% of

This article has been accepted for publication in a future issue of this journal, but has not been fully edited. Content may change prior to final publication. Citation information: DOI 10.1109/TIE.2015.2402114, IEEE Transactions on Industrial Electronics

the final value is given by the following expression [27]

$$t_s \approx 3.9\tau. \tag{26}$$

The rise time mainly depends on ω_n and can be approximated by [27]

$$t_r \approx 1.8/\omega_n. \tag{27}$$

B. Tuning by a Second Order Approximation

1) Tuning Objective: In wind turbine applications, the control of the grid-side converter is usually based on cascaded loops: outer loops, with slow dynamics, regulate the reactive power delivered to the grid and the dc-link voltage; they generate the references for the inner current controllers [6], [23]. A fast dynamics of the inner current loops is sought as they set the bottleneck of the whole system [3], [6], [8], [10]. Furthermore, a fast dynamics is also demanded to fulfill some stringent grid-code requirements [6], [8], [11]. In this scenario, a suitable design guideline points to minimize the current controller time constant τ, i.e., to maximize the decay rate of its dominant poles [8].

2) SISO Guideline Tuning Values: From the second order system defined by (20), some reference values can be obtained analytically. When the system is critically damped (i.e., $\xi = 1$) both eigenvalues coincide in a point, at which the real part of the dominant roots reaches a maximum value. This is given at

$$\alpha_{damp} = \frac{6 - 4\sqrt{2}}{t_d}. \tag{28}$$

This tuning would provide the tuning objective (minimization of τ), according to the SISO approximation.

From (20), it is possible to calculate the limit of stability as

$$\alpha_{lim} = \frac{2}{t_d}. \tag{29}$$

It is also interesting to define

$$\alpha_{10\%} = \frac{2\pi f_s}{10} \tag{30}$$

as the gain that corresponds with the one-to-ten limit in the bandwidth over control frequency ratio [1], [7]. This high-bandwidth tuning provides a fast rise time, but with undamped response (overshoot) [18].

V. Dynamics Assessment and Tuning by MIMO Root Locus

The previous section shows how to simplify the dynamics to a second order non-minimum phase system. However, that analysis assumes the coupling terms are negligible, which is not accurate, specially when considering a low-sampling-frequency constraint. This section provides a methodology for eigenvalues calculation taking into account the non-diagonal terms arising from the MIMO modeling with system delays.

A. MIMO Poles and Zeros

Firstly, MIMO poles and zeros of $\mathbf{G}(s)$ and $\mathbf{K}(s)$ are calculated. The following remarks should be pointed out.

- A MIMO transfer function matrix has a pole at p_0 if any of its elements has a pole at p_0 [19], [20].
- MIMO zeros are such z_0 values at which the MIMO matrix loses rank [19], [20]. Usually, they do not correspond with zeros of sensitivity-matrix elements [19], [20].

It is recommended to set each matrix in its Smith-McMillan form to find poles and zeros, and their multiplicities [19], [20]. The Smith-McMillan form of $\mathbf{G}(s)$, obtained according to the guidelines in [19], [20], is

$$\mathbf{G}^{SM}(s) = \begin{bmatrix} -s + \frac{2}{t_d} & 0 \\ 0 & \frac{-s+\frac{2}{t_d}}{(s+\frac{R}{L})^2(s+\frac{2}{t_d})^2+4\omega^2 s^2} \end{bmatrix}. \tag{31}$$

From (31), $\mathbf{G}(s)$ has a double (non-minimum phase) zero at $+2/t_d$. Approximated values for $\mathbf{G}(s)$ poles can be obtained by assuming $2/t_d >> R/L \sim \omega$ (circuit time constants are longer than the time-delay [3]), so

$$\begin{aligned} p_{p1,p2} &\approx -\frac{R}{L}(1 \pm j t_d \omega) \qquad \text{(plant complex pair of poles)} \\ p_{t1,t2} &\approx -\frac{2}{t_d} \pm j2\omega \qquad \text{(time-delay complex pair of poles).} \end{aligned} \tag{32}$$

$\mathbf{K}(s)$ is Smith-McMillan by definition: it has a double pole at the origin and a double zero at $-R/L$.

B. MIMO Eigenvalues Calculation

The sensitivity matrix is defined by

$$\mathbf{S}(s) = [\mathbf{I} + \mathbf{G}(s)\mathbf{K}(s)]^{-1}. \tag{33}$$

The MIMO poles of (33) define the dynamics of the closed-loop system. E.g., all of them should be in the left-half-plane to assure stability.

Since the product $\mathbf{G}(s)\mathbf{K}(s)$ does not contain unstable MIMO pole-zero cancellations (this can be checked from MIMO poles and zeros calculation in Section V-A), all the closed-loop system poles defining dynamic responses are given by the roots of the characteristic polynomial [19], [20], i.e.,

$$\det[\mathbf{S}^{-1}(s)] = \det[\mathbf{I} + \mathbf{G}(s)\mathbf{K}(s)] = 0. \tag{34}$$

As in the SISO case, the root-locus given by (34) depends on α (gain). Therefore, the tuning gain that provides faster decaying dominant roots can be identified by inspection of root-locus diagrams.

To ease the calculations (and avoid any possible unstable pole-zero cancellation), the characteristic polynomial (34) is re-written using Matrix Fraction Description (MFD) matrices [19], as follows:

$$\det[\mathbf{S}^{-1}(s)] = \det[\bar{\mathbf{G}}_D(s)\mathbf{K}_D(s) + \bar{\mathbf{G}}_N(s)\mathbf{K}_N(s)] = 0 \tag{35}$$

This article has been accepted for publication in a future issue of this journal, but has not been fully edited. Content may change prior to final publication. Citation information: DOI 10.1109/TIE.2015.2402114, IEEE Transactions on Industrial Electronics

with

$$\begin{aligned}
\bar{\mathbf{G}}_D(s) &= L[(s+R/L)^2(s+2/t_d)^2+4\omega^2 s^2]\mathbf{I}\\
\bar{\mathbf{G}}_N(s) &= (-s+2/t_d)\\
&\quad\begin{bmatrix}(s+R/L)(s+2/t_d) & -2\omega s\\ 2\omega s & (s+R/L)(s+2/t_d)\end{bmatrix}\\
\mathbf{K}_D(s) &= s\mathbf{I}\\
\mathbf{K}_N(s) &= \alpha L(s+R/L)\mathbf{I}.
\end{aligned} \tag{36}$$

1) Computer Aided Calculation: In practice, it is very cumbersome to handle (36), since it involves non-diagonal matrix determinant calculations. This means high order expressions, which are very difficult to simplify. On the other hand, "Geometric Analysis" for MIMO systems has also been discarded because of its complexity due to α^2 terms in (34)–(35), as reported in [28].

Thus, in this paper, the problem has been solved by means of a computer-aided methodology. By means of the Matlab Symbolic Math toolbox, the characteristic equation from (34)–(36) results in a sixth order expression as follows

$$\begin{aligned}
\det(\mathbf{S}^{-1}) &= L^2t_d^2s^6+(-2\alpha L^2t_d^2+4L^2t_d+2RLt_d^2)s^5\\
&\quad+(L^2\alpha^2t_d^2+16L^2t_d^2\omega^2+4L^2-4LR\alpha t_d^2\\
&\quad+8LRt_d+R^2t_d^2)s^4+(-4L^2\alpha^2t_d+8L^2\alpha\\
&\quad+2LR\alpha^2t_d^2+8LR-2R^2\alpha t_d^2+4R^2t_d)s^3\\
&\quad+(4L^2\alpha^2-8LR\alpha^2t_d+16LR\alpha+R^2\alpha^2t_d^2\\
&\quad+4R^2)s^2+(-4t_dR^2\alpha^2+8R^2\alpha+8LR\alpha^2)s\\
&\quad+4R^2\alpha^2=0.
\end{aligned} \tag{37}$$

Subsequently, the solutions are calculated and depicted as function of α (parametric analysis) for a wide range of α values. Fig. 4 shows a generic root locus obtained by solving (37) for increasing α values. Section V-C details how to interpret the MIMO root-locus diagrams.

It is also interesting to note that (37) is a function of ω. This dependence comes from the cross-coupling terms in the plant modeling. In a grid-connected converter, ω can be assumed to be constant. However, in order to extend the proposed methodology to motor drives, a parametric analysis as a function of ω should be also considered, as this parameter depends on the machine speed [15]–[17].

C. Tuning by MIMO Root-Locus Diagrams

Fig. 4 describes a generic root locus obtained by solving (37) for increasing α values. The following assumptions are made in order to analyze the MIMO root-locus diagram.

- The closed-loop poles are complex pairs. At $\alpha = 0\,\mathrm{rad/s}$ the poles correspond to $\mathbf{G}(s)\mathbf{K}(s)$ in open loop. As α increases, the pole-trajectories tend to $-R/L$, (plant), $2/t_d$ (delay) and ∞, which correspond to MIMO zeros.
- As shown in the zoomed region of Fig. 4, the eigenvalues from trajectory-1 are very close to the double zero at $-R/L$ [imposed by control design in (7)]. This implies a double pole-zero cancellation around $-R/L$ [19], [20], and hence, the effect of these eigenvalues is not dominant in the presence of a current step.
- At the range of gains suitable for tuning (i.e., up to $\alpha_{10\%}$, see shaded region in Fig. 4), the poles of trajectory-3 are faster than the ones of trajectory-2. Therefore, they are less dominant in the time response and hence, they are neglected.
- The trajectory-2 poles set the system dynamics, as they are dominant. Therefore, the dominant poles $p_{d_{1,2}}$ are re-defined accordingly as the eigenvalues given by the trajectory-2 in the MIMO root locus.
- The expressions (22)–(27), as defined in Section IV for a standard second order system (including the non-minimum phase zero at $-2/t_d$), are suitable to describe the dynamics, but according to the re-defined MIMO dominant eigenvalues .

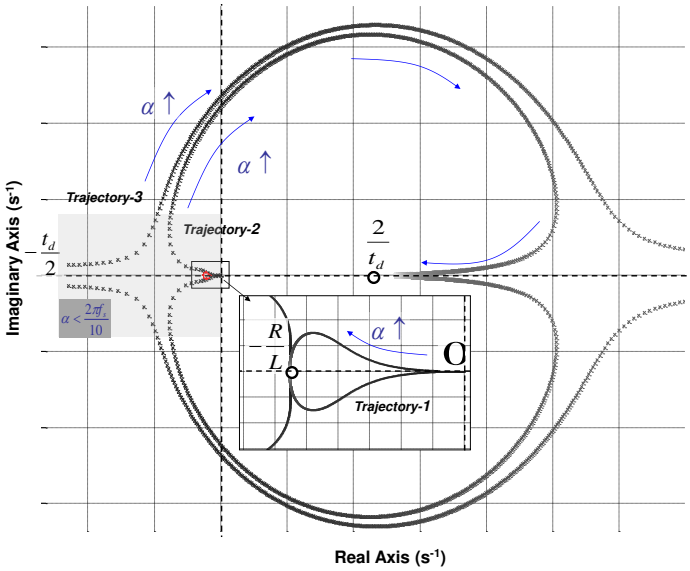

Fig. 4. Root locus given by (34)-(37) for increasing values of α.

As detailed in section IV-B1, the proposed tuning method aims to minimize the current control time constant. This is achieved by maximizing the negative real part of the dominant eigenvalues: by inspection of the MIMO root locus it is possible to select the tuning that places $p_{d_{1,2}}$ (trajectory-2) as far as possible from the RHP. This key tuning is then defined as α_{min_τ}.

VI. Experimental Verification

The theoretical analysis has been validated in a lab-scale prototype. The digital control is executed in a dSpace MABXII DS1401 platform.

Fig. 5 shows the control scheme and a photo of the test-bed. The control algorithm is as follows: the i_d controller is an inner loop of the dc-link voltage U_{dc} outer loop. The reactive current i_q is directly set by the dSpace user interface, so the key waveforms are obtained by triggering step changes in the reactive current reference i_q^* [8]. The power converter is working in rectifier mode of operation, which permits to test the performance of the current controllers (suitable for

This article has been accepted for publication in a future issue of this journal, but has not been fully edited. Content may change prior to final publication. Citation information: DOI 10.1109/TIE.2015.2402114, IEEE Transactions on Industrial Electronics

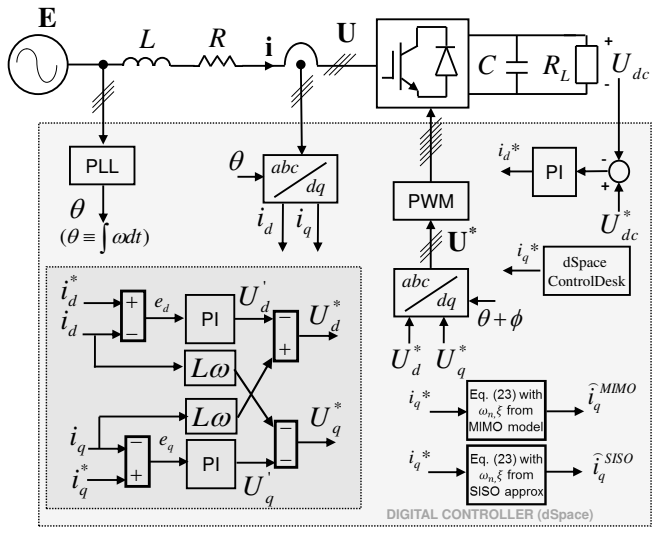

(a)

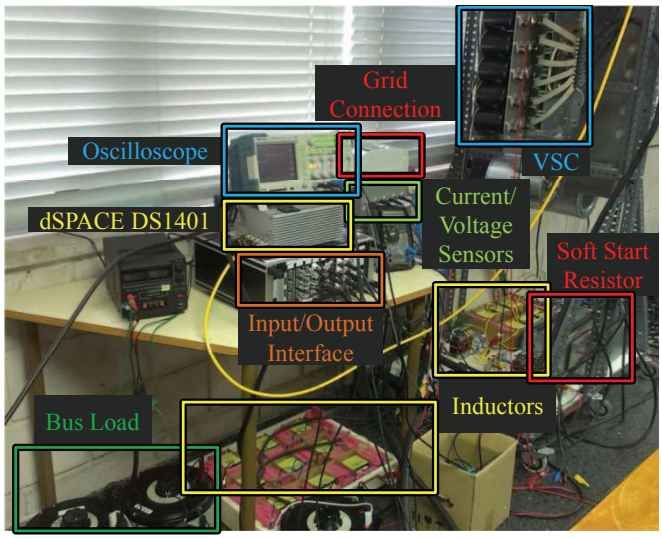

(b)

Fig. 5. Lab prototype setup. (a) Circuit and (active-rectifier) controller implementation; (b) Photo.

any working point of the power converter) without needing an external power source.

Two different sampling frequencies have been considered in the tests: $f_s = 2850\,\text{Hz}$ and $f_s = 1500\,\text{Hz}$. As the switching carrier frequency f_c is reduced, it causes more significant low order harmonics (in practical applications, f_s is reduced as a result of reducing f_c and switching losses). The setup circuit includes large inductors to better filter switching harmonics. Grid voltage harmonics and dead-time effects are also an important source of distortion at low f_s (i.e., as the control bandwidths are reduced accordingly). Therefore, a selective active filtering was implemented aiming to enhance steady-state waveforms without impairing very much the transient response assessment (see Section VI-C2). For each of the two cases, the equivalent resistance in the plant model of the current loop, which includes the effects associated to the switching and conduction losses, has been previously

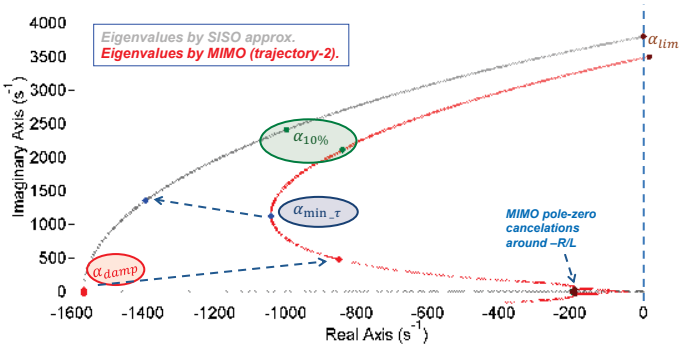

Fig. 6. Detail of MIMO and SISO Root loci for $f_s = 2850\,\text{Hz}$ setup.

estimated by the method presented in [29].

Besides current distortion, another practical issue which difficulties the assessment of experimental figures is the inherent low resolution of the problem: the time constant (a parameter to measure) and the sampling period $1/f_s$ are of the same order of magnitude. To support time-domain assessments, the estimated currents $\hat{i}_q^{\text{SISO}}$ and $\hat{i}_q^{\text{MIMO}}$ are depicted. These are the estimated dominant time responses, which are obtained by applying the same current step as that commanded to the actual plant to (23), with the corresponding set of parameters ω_n and ξ, as shown in Fig. 5(a). It should be also noticed that the non-minimum phase zero at the numerator of (23) causes some inaccuracies at the very beginning of the transient [19], as discussed in Section III-A.

A. Case A: Tests at $f_s = 2850\,\text{Hz}$

The setup parameters are shown in Table I. Fig. 6 details the position of the dominant poles (the root loci is zoomed at the second quadrant for a better resolution; the MIMO trajectory-3 is not displayed as its eigenvalues are not dominant). Table II summarizes the main parameters in Fig. 6 for both the SISO and the MIMO approaches. The key values (highlighted in the plot) and assumptions to be made are explained below.

- The eigenvalues provided by the SISO approximation are faster and more damped than the ones provided by the MIMO solution, since the latter quantifies the effect of the coupling terms. This cross coupling is expected to be noticeable during transients.
- The tuning at α_{damp} corresponds to the theoretical value from (28). It theoretically fulfills the tuning objective according to the SISO approximation. However, it corresponds to a quite reduced gain in the MIMO root locus.
- The tuning at α_{min_τ} is obtained by inspection of the MIMO root locus (the α which maximizes the negative real part of the eigenvalues). This is achieved with a gain higher than α_{damp}.
- The tuning at $\alpha_{10\%}$ is selected according to the one-to-tenth rule $\alpha_{10\%} = 2\pi f_s/10$.

Fig. 7 shows the test results for the selected tunings. Table III shows the integral absolute error (IAE) from Fig. 7

This article has been accepted for publication in a future issue of this journal, but has not been fully edited. Content may change prior to final publication. Citation information: DOI 10.1109/TIE.2015.2402114, IEEE Transactions on Industrial Electronics

TABLE I
CASE A: EXPERIMENTAL SETUP CIRCUIT PARAMETERS

Parameter	Value
Plant Inductance	$L = 12.5\,\text{mH}$
Estimated Plant Resistance	$R = 2.2\,\Omega$
Sampling frequency	$f_s = 2850\,\text{Hz}$
Carrier frequency	$f_c = 2850\,\text{Hz}$
$t_d = 1.5/f_s$	$351\,\mu\text{s}$
R_L	$255\,\Omega$
Dc-link voltage	$U_{dc} = 700\,\text{V}$
Fundamental angular frequency	$\omega = 2\pi 50\,\text{rad/s}$

TABLE II
PREDICTED DYNAMICS FROM SISO AND MIMO ROOT LOCUS DIAGRAMS OF FIG. 6

Tuning at $\alpha = \alpha_{damp} = 652\,\text{rad/s}$		
SISO	$p_d = -1574\,\text{rad/s}$	$\tau = 635\,\mu\text{s}$ (1^{st} order) $t_{st} \approx 2.5\,\text{ms}$
MIMO	$p_{d_{1,2}} = -857 \pm j480\,\text{rad/s}$	$\omega_n = 982\,\text{rad/s}$ $\xi = 0.87$ $t_{st} \approx 4.6\,\text{ms}$
Tuning at $\alpha = \alpha_{min\_\tau} = 1000\,\text{rad/s}$		
SISO	$p_{d_{1,2}} = -1400 \pm j1356\,\text{rad/s}$	$\omega_n = 1950\,\text{rad/s}$ $\xi = 0.72$ $t_{st} \approx 2.9\,\text{ms}$
MIMO	$p_{d_{1,2}} = -1048 \pm j1127\,\text{rad/s}$	$\omega_n = 1540\,\text{rad/s}$ $\xi = 0.68$ $t_{st} \approx 3.8\,\text{ms}$
Tuning at $\alpha = \alpha_{10\%} = 1791\,\text{rad/s}$		
SISO	$p_{d_{1,2}} = -1005 \pm j2407\,\text{rad/s}$	$\omega_n = 2609\,\text{rad/s}$ $\xi = 0.39$ $t_{st} \approx 4.0\,\text{ms}$
MIMO	$p_{d_{1,2}} = -848 \pm j2121\,\text{rad/s}$	$\omega_n = 2284\,\text{rad/s}$ $\xi = 0.37$ $t_{st} \approx 4.7\,\text{ms}$

captures, obtained by

$$\text{IAE} = \sum_{t=0}^{t_\text{w}} \frac{|i_q - \hat{i}_q|}{f_s} \tag{38}$$

with $t_\text{w} = 10\,\text{ms}$ being the time window of the oscilloscope captures [18], [29].

From these results, it can be observed that $\widehat{i}_q^{\text{MIMO}}$ matches well the measured current i_q in all the cases. More specifically, Fig. 7(e) proves that the minimum time constant is achieved with α_{min_τ}, as correctly predicted by the MIMO root locus. The corresponding IAEs in Table III show that the MIMO prediction matches better than the SISO one the actual response with α_{min_τ} and α_{damp}. From Fig. 7(d), and its corresponding IAEs, $\widehat{i}_q^{\text{SISO}}$ is less accurate than $\widehat{i}_q^{\text{MIMO}}$ with α_{damp} being the tuning gain. These results using low tuning gains also prove that the SISO approximation is not suitable to find the aimed gain, which minimizes the dominant time constant. At high tuning gains, both SISO and MIMO time-domain predictions become similar [see Fig. 7(f) and the last rows in Table III]. This fact is also as expected from Fig. 6 (SISO and MIMO trajectories tend to be closer as α increases) and their estimated settling times in Table II.

TABLE III
IAE OBTAINED FROM THE EXPERIMENTAL TESTS OF FIG. 7

Tuning at $\alpha = \alpha_{damp} = 652\,\text{rad/s}$	
SISO	$\text{IAE} = 4.9E^{-3}\,\text{A}\cdot\text{s}$
MIMO	$\text{IAE} = 1.0E^{-3}\,\text{A}\cdot\text{s}$
Tuning at $\alpha = \alpha_{min\_\tau} = 1000\,\text{rad/s}$	
SISO	$\text{IAE} = 1.8E^{-3}\,\text{A}\cdot\text{s}$
MIMO	$\text{IAE} = 0.8E^{-3}\,\text{A}\cdot\text{s}$
Tuning at $\alpha = \alpha_{10\%} = 1791\,\text{rad/s}$	
SISO	$\text{IAE} = 3.5E^{-3}\,\text{A}\cdot\text{s}$
MIMO	$\text{IAE} = 3.4E^{-3}\,\text{A}\cdot\text{s}$

TABLE IV
CASE B: EXPERIMENTAL SETUP CIRCUIT PARAMETERS

Parameter	Value
Plant Inductance	$L = 24.3\,\text{mH}$
Estimated Plant Resistance	$R = 1.7\,\Omega$
Sampling frequency	$f_s = 1500\,\text{Hz}$
Carrier frequency	$f_c = 1500\,\text{Hz}$
$t_d = 1.5/f_s$	$1\,\text{ms}$
R_L	$255\,\Omega$
Dc-link voltage	$U_{dc} = 700\,\text{V}$
Fundamental angular frequency	$\omega = 2\pi 50\,\text{rad/s}$

B. Case B: Tests at $f_s = 1500\,\text{Hz}$

The setup parameters are shown in Table IV. Fig. 8 displays the root loci from MIMO and SISO approaches, while Table V details the position of the dominant poles for the three key tunings, which have been obtained as in Case A.

Fig. 9 shows the key results for the selected tunings and Table VI their corresponding IAEs. Since the main controller bandwidth is reduced very much, the selective harmonic elimination controller (see Section VI-C2) has some influence on the dynamics: a good filtering is achieved in steady state, but the 6^{th} harmonic oscillation arises during the transients. This fact impairs the assessments and significantly increases the IAEs (with respect to the ones of Section VI-A). Despite the 6^{th} harmonic ripple, it can be said that $\widehat{i}_q^{\text{MIMO}}$ correctly predicts the dominant time constant in all the cases. As expected, the dominant time constant is minimized with α_{min_τ} being the tuning gain. The experiments using α_{damp} should be also highlighted: Fig. 9(d) and its corresponding IAEs prove that $\widehat{i}_q^{\text{MIMO}}$ fits much better than $\widehat{i}_q^{\text{SISO}}$ the actual i_q current. Therefore, the results using α_{min_τ} and α_{damp} also show that the SISO approximation is not suitable to find the gain that minimizes the dominant time constant. As also predicted in Fig. 8, SISO and MIMO time-domain predictions become similar when using high tuning gains.

C. Implementation Issues

1) Discretization of Integrators: Similarly to the analysis in section III-A, the accuracy of the time domain implementation in the range of frequencies of the control should be checked. Fig. 10 shows the frequency response of the discrete-time integrator implementation obtained by the Tustin method. It can be observed that it matches the theoretical frequency response up to $f_s/10$ and beyond. At higher frequencies, the magnitude response of the discretized integrator becomes

This article has been accepted for publication in a future issue of this journal, but has not been fully edited. Content may change prior to final publication. Citation information: DOI 10.1109/TIE.2015.2402114, IEEE Transactions on Industrial Electronics

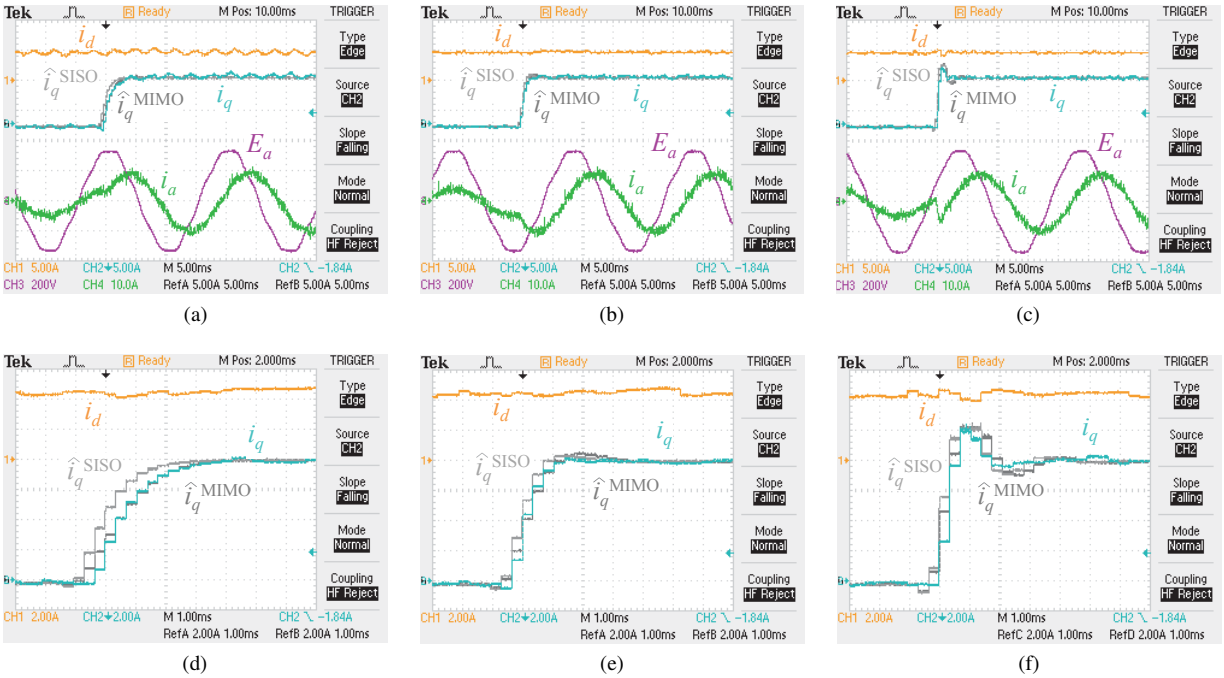

Fig. 7. Step responses from $i_q^* = 0$ to $i_q^* = -8$ A at $f_s = 2850$ Hz for different tunings. (a) $\alpha = \alpha_{damp}$; (b) $\alpha = \alpha_{min\_\tau}$; (c) $\alpha = \alpha_{10\%}$; (d) $\alpha = \alpha_{damp}$, zoomed view; (e) $\alpha = \alpha_{min\_\tau}$, zoomed view; (f) $\alpha = \alpha_{10\%}$, zoomed view. Note that i_q, $\widehat{i}_q^{\text{SISO}}$ and $\widehat{i}_q^{\text{MIMO}}$ are inverted.

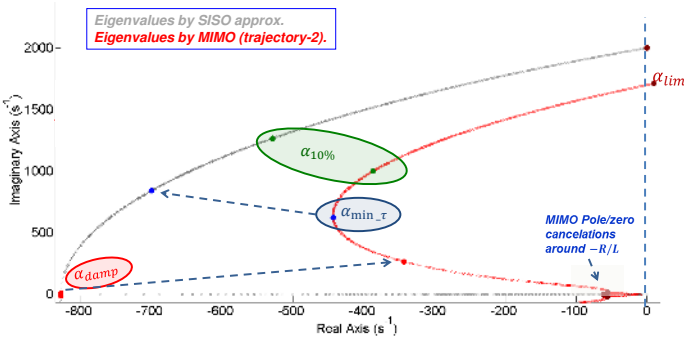

Fig. 8. MIMO and SISO Root-loci for $f_s = 1500Hz$ setup.

TABLE V
PREDICTED DYNAMICS FROM SISO AND MIMO ROOT LOCUS DIAGRAMS OF FIG. 8

Tuning at $\alpha = \alpha_{damp} = 343\,\text{rad/s}$		
SISO	$p_d = -828\,\text{rad/s}$	$\tau = 635\,\mu\text{s}$ (1^{st} order) $t_{st} \approx 4.7\,\text{ms}$
MIMO	$p_{d_{1,2}} = -364 \pm j247\,\text{rad/s}$	$\omega_n = 440\,\text{rad/s}$ $\xi = 0.83$ $t_{st} \approx 10.7\,\text{ms}$
Tuning at $\alpha = \alpha_{min\_\tau} = 600\,\text{rad/s}$		
SISO	$p_{d_{1,2}} = -700 \pm j843\,\text{rad/s}$	$\omega_n = 828\,\text{rad/s}$ $\xi = 0.64$ $t_{st} \approx 5.6\,\text{ms}$
MIMO	$p_{d_{1,2}} = -464 \pm j616\,\text{rad/s}$	$\omega_n = 771\,\text{rad/s}$ $\xi = 0.60$ $t_{st} \approx 8.4\,\text{ms}$
Tuning at $\alpha = \alpha_{10\%} = 963\,\text{rad/s}$		
SISO	$p_{d_{1,2}} = -529 \pm j1267\,\text{rad/s}$	$\omega_n = 1373\,\text{rad/s}$ $\xi = 0.39$ $t_{st} \approx 7.4\,\text{ms}$
MIMO	$p_{d_{1,2}} = -402 \pm j997\,\text{rad/s}$	$\omega_n = 1075\,\text{rad/s}$ $\xi = 0.37$ $t_{st} \approx 9.7\,\text{ms}$

lower than the one of the ideal integrator, so a good high-frequency noise attenuation is expected. It is worth remarking that (23), which is used to estimate $\widehat{i}_q^{\text{SISO}}$ and $\widehat{i}_q^{\text{MIMO}}$ in Fig. 5(a), is also discretized by the Tustin method.

2) Active Filtering for Dead-Time and Grid Harmonics: As the sampling frequency and achievable control bandwidth are reduced, grid voltage harmonics and dead-time effects become very significant. In order to deal with current distortion, selective resonant filters for fifth (negative sequence) and seventh (positive sequence) harmonics have been implemented in parallel to the main $dq-PI$ controller [30]. Each resonant filter has been implemented with a very small gain, and each phase-lead compensation angle is calculated according to the Nyquist criterion, as explained in [31]. This implementation eliminates steady-state distortion due to grid harmonics and dead-times. However, some oscillation is present during transients: a sixth order harmonic oscillation in the $dq-$frame (i.e., at resonant frequencies, the Nyquist trajectories are closer to the critical point [31]). This oscillation becomes more significant as f_s is reduced, and hence impairs experimental validations, as shown in Section VI-B. This corresponds with the fact that the disturbance rejection ability decreases with the controller bandwidth [3].

VII. CONCLUSIONS

This paper presents a systematic procedure for accurate dynamics assessment and tuning of dq-PI current controllers when a low sampling frequency is an imposed constraint.

This article has been accepted for publication in a future issue of this journal, but has not been fully edited. Content may change prior to final publication. Citation information: DOI 10.1109/TIE.2015.2402114, IEEE Transactions on Industrial Electronics

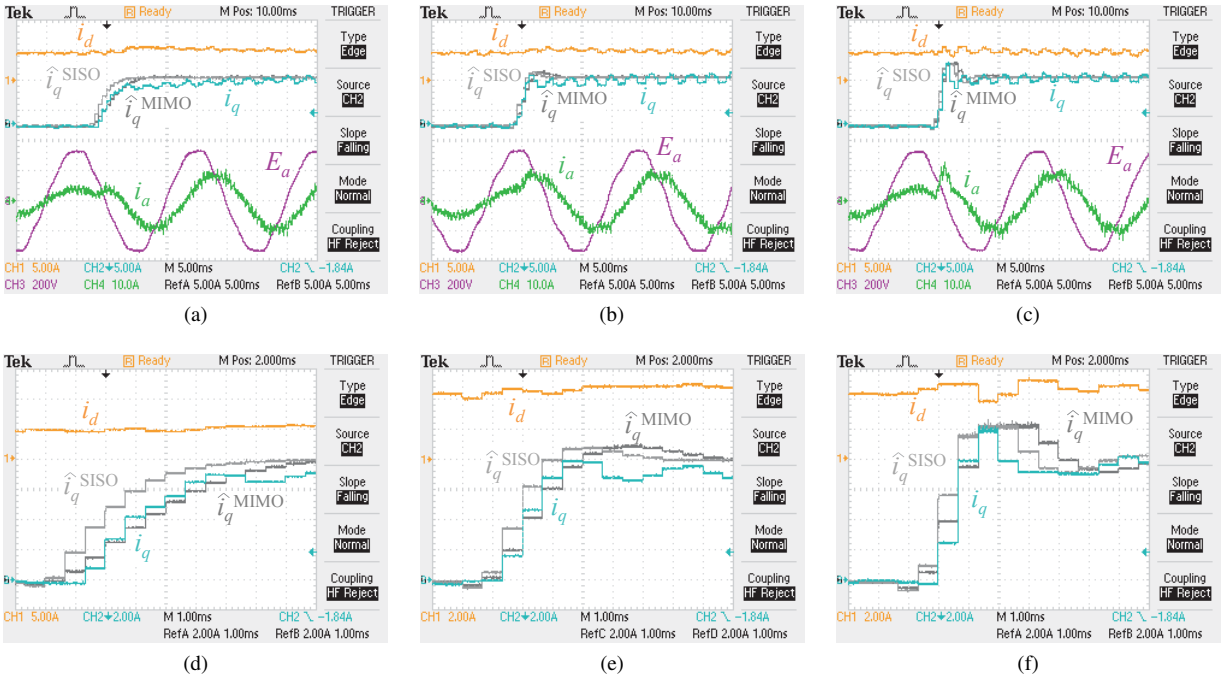

Fig. 9. Step responses from $i_q^* = 0$ to $i_q^* = -8$ A at $f_s = 1500$ Hz for different tunings. (a) $\alpha = \alpha_{damp}$; (b) $\alpha = \alpha_{min\_\tau}$; (c) $\alpha = \alpha_{10\%}$; (d) $\alpha = \alpha_{damp}$, zoomed view; (e) $\alpha = \alpha_{min\_\tau}$, zoomed view; (f) $\alpha = \alpha_{10\%}$, zoomed view. Note that i_q, $\hat{i}_q^{\text{SISO}}$ and $\hat{i}_q^{\text{MIMO}}$ are inverted.

TABLE VI
IAE OBTAINED FROM THE EXPERIMENTAL TESTS OF FIG. 9

Tuning at $\alpha = \alpha_{damp} = 343\,\text{rad/s}$	
SISO	$\text{IAE} = 13.3E^{-3}\,\text{A}\cdot\text{s}$
MIMO	$\text{IAE} = 4.8E^{-3}\,\text{A}\cdot\text{s}$
Tuning at $\alpha = \alpha_{min\_\tau} = 600\,\text{rad/s}$	
SISO	$\text{IAE} = 6.6E^{-3}\,\text{A}\cdot\text{s}$
MIMO	$\text{IAE} = 6.4E^{-3}\,\text{A}\cdot\text{s}$
Tuning at $\alpha = \alpha_{10\%} = 963\,\text{rad/s}$	
SISO	$\text{IAE} = 7.9E^{-3}\,\text{A}\cdot\text{s}$
MIMO	$\text{IAE} = 8.1E^{-3}\,\text{A}\cdot\text{s}$

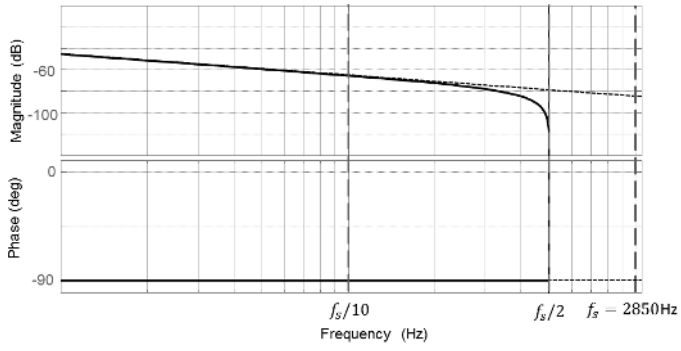

Fig. 10. Accuracy of the discrete-time integrator obtained by the Tustin method. Solid: discrete-time implementation ($H(z) = \frac{1}{2f_s}\frac{z+1}{z-1}$). Dotted: ideal integator ($H(s) = 1/s$).

This contribution specially aims to grid-connected converters in renewable energy applications, in which a fast dynamics is needed, while the sampling frequency tends to decrease as power ratings increase (e.g., grid code requirements in multi-MW wind turbines). Taking into consideration cascaded-control structures and grid-code requirements, minimizing the current controller time constant is proposed as the tuning objective.

The theoretical approach firstly models the system taking the system delays and coupling terms into consideration. Subsequently, a SISO root-locus approximation is obtained by neglecting the coupling terms, as usually assumed. However, this assumption tends to become inaccurate for low sampling frequency. A MIMO root locus based approach is then proposed to provide a more accurate calculation of the dominant eigenvalues. Then, by inspection of MIMO root locus diagrams, the gain which minimizes the current controller time constant α_{min_τ} is obtained.

Experimental verification validates the high accuracy of the proposed tuning methodology. Experimental figures prove that α_{min_τ} minimizes the settling time, and hence the current loop time constant. Besides the tuning objective is suitable from the MIMO root locus method, it is also important to highlight how real dynamics tends to be slower and more undamped than predictions assuming a negligible cross coupling.

REFERENCES

[1] L. Harnefors and H.-P. Nee, "Model-based current control of AC machines using the internal model control method," *IEEE Trans. Ind. Appl.*, vol. 34, no. 1, pp. 133–141, Jan./Feb. 1998.

[2] F. Briz, M. Degner, and R. Lorenz, "Dynamic analysis of current regulators for AC motors using complex vectors," *IEEE Trans. Ind. Appl.*, vol. 35, no. 6, pp. 1424–1432, Nov./Dec. 1999.

[3] D. G. Holmes, T. A. Lipo, B. McGrath, and W. Kong, "Optimized design of stationary frame three phase AC current regulators," *IEEE Trans. Power Electron.*, vol. 24, no. 11, pp. 2417–2426, Nov. 2009.

[4] B. Bahrani, A. Karimi, B. Rey, and A. Rufer, "Decoupled DQ-current control of grid-tied voltage source converters using nonparametric models," *IEEE Trans. Ind. Electron.*, vol. 60, no. 4, pp. 1356–1366, Apr. 2013.

[5] B. Bahrani, M. Vasiladiotis, and A. Rufer, "High-order vector control of grid-connected voltage-source converters with LCL-filters," *IEEE Trans. Ind. Electron.*, vol. 61, no. 6, pp. 2767–2775, Jun. 2014.

[6] A. Timbus, M. Liserre, R. Teodorescu, P. Rodriguez, and F. Blaabjerg, "Evaluation of Current Controllers for Distributed Power Generation Systems," *IEEE Trans. Power Electron.*, vol. 24, no. 3, pp. 654–664, Mar. 2009.

[7] S. Buso and P. Mattavelli, *Digital Control in Power Electronics*. Morgan and Claypool, 2006, pp. 25–30, 46–61, 93–98, 103–107.

[8] A. Vidal, F. D. Freijedo, A. G. Yepes, P. Fernandez-Comesana, J. Malvar, O. Lopez, and J. Doval-Gandoy, "Assessment and optimization of the transient response of proportional-resonant current controllers for distributed power generation systems," *IEEE Trans. Ind. Electron.*, vol. 60, no. 4, pp. 1367–1383, Apr. 2013.

[9] J.-W. Chui and S.-K. Sui, "New current control concept-minimum time current control in the three-phase PWM converter," *IEEE Trans. Power Electron.*, vol. 12, no. 1, pp. 124–131, 1997.

[10] K. Astrom and T. Hagglund, *PID Controllers: Theory, Design and Tuning.* Instrument Society of America, 1995, pp. 274–279.

[11] A. Camacho, M. Castilla, J. Miret, A. Borrell, and L. de Vicuna, "Active and reactive power strategies with peak current limitation for distributed generation inverters during unbalanced grid faults," *IEEE Trans. Ind. Electron.*, to be published.

[12] K. Ma and F. Blaabjerg, "Thermal optimised modulation methods of three-level neutral-point-clamped inverter for 10 MW wind turbines under low-voltage ride through," *IET Power Electron.*, vol. 5, no. 6, pp. 920–927, Jul. 2012.

[13] K. Ma, M. Liserre, and F. Blaabjerg, "Operating and loading conditions of a three-level neutral-point-clamped wind power converter under various grid faults," *IEEE Trans. Ind. Appl.*, vol. 50, no. 1, pp. 520–530, 2014.

[14] L. Harnefors, "Modeling of three-phase dynamic systems using complex transfer functions and transfer matrices," *IEEE Trans. Ind. Electron.*, vol. 54, no. 4, pp. 2239–2248, Aug. 2007.

[15] J. Holtz, J. Quan, J. Pontt, J. Rodriguez, P. Newman, and H. Miranda, "Design of fast and robust current regulators for high-power drives based on complex state variables," *IEEE Trans. Ind. Appl.*, vol. 40, no. 5, pp. 1388–1397, Sep./Oct. 2004.

[16] J.-S. Yim, S.-K. Sul, B.-H. Bae, N. R. Patel, and S. Hiti, "Modified current control schemes for high-performance permanent-magnet ac drives with low sampling to operating frequency ratio," *IEEE Trans. Ind. Appl.*, vol. 45, pp. 763–770, Mar./Apr. 2009.

[17] H. Kim, M. Degner, J. Guerrero, F. Briz, and R. Lorenz, "Discrete-time current regulator design for AC machine drives," *IEEE Trans. Ind. Appl.*, vol. 46, no. 4, pp. 1425–1435, Jul./Aug. 2010.

[18] A. G. Yepes, A. Vidal, J. Malvar, O. Lopez, and J. Doval-Gandoy, "Tuning method aimed at optimized settling time and overshoot for synchronous proportional-integral current control in electric machines," *IEEE Trans. Power Electron.*, pp. 3041–3054, Jun. 2014.

[19] G. C. Goodwin, S. F. Graebe, and M. E. Salgado, *Control System Design*. Prentice Hall, 2000, pp. 80–81, 98–99, 178–189, 594–597, 603–608.

[20] S. Skogestad and I. Postlethwaite, *Multivariable Feedback Control*. Wiley, 2005, pp. 27, 67–71, 119–154.

[21] L. Harnefors, L. Zhang, and M. Bongiorno, "Frequency-domain passivity-based current controller design," *IET Power Electron.*, vol. 1, no. 4, pp. 455–465, Dec. 2008.

[22] R. Turner, S. Walton, and R. Duke, "A case study on the application of the nyquist stability criterion as applied to interconnected loads and sources on grids," *IEEE Trans Ind Electron*, vol. 60, no. 7, pp. 2740–2749, Jul. 2013.

[23] R. Teodorescu and F. Blaabjerg, "Flexible control of small wind turbines with grid failure detection operating in stand-alone and grid-connected mode," *IEEE Trans. Power Electron.*, vol. 19, no. 5, pp. 1323–1332, 2004.

[24] M. Liserre, R. Teodorescu, and F. Blaabjerg, "Stability of photovoltaic and wind turbine grid-connected inverters for a large set of grid impedance values," *IEEE Trans. Power Electron.*, vol. 21, no. 1, pp. 263–272, 2006.

[25] A. Petersson, L. Harnefors, and T. Thiringer, "Evaluation of current control methods for wind turbines using doubly-fed induction machines," *IEEE Trans. Power Electron.*, vol. 20, no. 1, pp. 227–235, Jan. 2005.

[26] J. Espi, J. Castello, R. Garcia-Gil, G. Garcera, and E. Figueres, "An adaptive robust predictive current control for three-phase grid-connected inverters," *IEEE Trans. Ind. Electron.*, vol. 58, no. 8, pp. 3537–3546, 2011.

[27] R. S. Burns, *Advanced Control Engineering*. Butterworth-Heinemann, 2001, pp. 57–58,118–132.

[28] B. Newman and D. Fu, "Sketching rules for the multivariable root locus design technique," in *Proc. American Control Conference*, Philadelphia (USA), Jun. 1998.

[29] A. Vidal, A. Yepes, F. Freijedo, J. Malvar, O. Lopez, and J. Doval-Gandoy, "A technique to estimate the equivalent loss resistance of grid-tied converters for current control analysis and design," *IEEE Trans. Power Electron.*, vol. 30, no. 3, pp. 1747–1761, 2015.

[30] C. Busada, S. Gomez Jorge, A. Leon, and J. Solsona, "Current controller based on reduced order generalized integrators for distributed generation systems," *IEEE Trans. Ind. Electron.*, vol. 59, no. 7, pp. 2898–2909, 2012.

[31] A. Yepes, F. Freijedo, O. Lopez, and J. Doval-Gandoy, "Analysis and design of resonant current controllers for voltage source converters by means of nyquist diagrams and sensitivity function," *IEEE Trans. Ind. Electron.*, vol. 58, no. 11, pp. 5231 – 5250, 2011.

Francisco D. Freijedo received the M.Sc. degree in Physics from the University of Santiago de Compostela, Santiago de Compostela, Spain, in 2002 and the Ph.D. degree from the University of Vigo, Vigo, Spain, in 2009. From 2005 to 2011, he was a Lecturer with the Department of Electronics Technology of the University of Vigo. From 2011 to 2014, he worked in the wind power industry as a control engineer. Since 2014, he is a Postdoctoral Researcher at the Department of Energy Technology of Aalborg University. His main research interests are in the areas of ac power conversion.

Ana Vidal (S'10) received the M.Sc. degree from the University of Vigo, Vigo, Spain, in 2010, where she is currently working toward the Ph.D. degree in the Applied Power Electronics Technology Research Group, University of Vigo. Since 2009, she has been with the Applied Power Electronics Technology Research Group. Her research interests include control of grid-connected converters and distributed power generation systems.

Alejandro G. Yepes (S'10-M'12) received the M.Sc. and the Ph.D. degree from University of Vigo, Vigo, Spain in 2009 and 2011, respectively. Since 2008, he is with the Applied Power Electronics Technology Research Group, University of Vigo. His main research interests include control of switching power converters and ac drives.

This article has been accepted for publication in a future issue of this journal, but has not been fully edited. Content may change prior to final publication. Citation information: DOI 10.1109/TIE.2015.2402114, IEEE Transactions on Industrial Electronics

Josep M. Guerrero (S01-M04-SM08-FM15) received the B.S. degree in telecommunications engineering, the M.S. degree in electronics engineering, and the Ph.D. degree in power electronics from the Technical University of Catalonia, Barcelona, in 1997, 2000 and 2003, respectively. Since 2011, he has been a Full Professor with the Department of Energy Technology, Aalborg University, Denmark, where he is responsible for the Microgrid Research Program. From 2012 he is a guest Professor at the Chinese Academy of Science and the Nanjing University of Aeronautics and Astronautics; and from 2014 he is chair Professor in Shandong University. His research interests is oriented to different microgrid aspects, including power electronics, distributed energy-storage systems, hierarchical and cooperative control, energy management systems, and optimization of microgrids and islanded minigrids. In 2014 he was awarded by Thomson Reuters as ISI Highly Cited Researcher, and in 2015 same year he was elevated as IEEE Fellow for contributions to distributed power systems and microgrids.

Jano Malvar (S10) received the M.Sc. degree from the University of Vigo, Vigo, Spain, in 2007, where he is currently working toward the Ph.D. degree in the Applied Power Electronics Technology Research Group, University of Vigo. Since 2007, he has been with the Applied Power Electronics Technology Research Group. His research focuses on power electronics, multiphase systems, ac drives and harmonics.

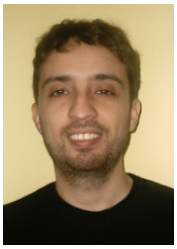

Oscar López (M'05) received the M.Sc. and the Ph.D. degree from University of Vigo, Vigo, Spain, in 2001 and 2009, respectively. Since 2004, he is an Assistant Professor at the University of Vigo. His research interests are in the areas of ac power switching converters technology.

Jesús Doval-Gandoy (M'99) received the M.Sc. degree from Polytechnic University of Madrid, Madrid, Spain, in 1991 and the Ph.D. degree from the University of Vigo, Vigo, Spain in 1999. From 1991 till 1994 he worked at industry. He is currently an Associate Professor at the University of Vigo. His research interests are in the areas of ac power conversion.